

# Theory and simulation of granular materials with hard spheres

Stefan Luding

**Abstract:** Granular Materials consist of particles that interact during contact, dissipate energy, and possibly rotate due to friction. Such discrete systems are examined with numerical simulations and, sometimes, can also be nicely described by theories like the kinetic theory or hydrodynamic continuum models. These days, great effort is invested to predict experimental observations quantitatively with simulations and theories.

One challenge in computational physics is thus to bridge the gap between the microscopic, “atomistic” simulations, and the macroscopic length scale of continuum models and experimental observation. First, an efficient algorithm for hard sphere molecular dynamics is presented, allowing for many-particle simulations of, e.g., granular systems. In the next step, a “micro-macro” transition is introduced which enables continuum quantities like the stress tensor to be accessed. The approach is used for dilute and dense dissipative granular gases, either freely cooling or heated with respect to the translational or rotational degrees of freedom.

**Keywords:** granular matter – event driven molecular dynamics – micro-macro transition – equation of state

## Contents

1	Introduction . . . . .	1
2	Model and Algorithm . . . . .	2
3	The Stress in dense granular gases . . . . .	4
4	The model for frictional and heated systems . . . . .	5
5	Mean field evolution equations . . . . .	6
6	Freely cooling granular media . . . . .	10
7	Micro-Macro Transition for a freely cooling system . . . . .	12
8	Summary and Conclusion . . . . .	13

## 1 Introduction

Granular materials are fascinating examples from the rich world of non-linear, dissipative, non-equilibrium systems [1–3]. Hard spheres, as a special case, are used also as

06. February 2003

Stefan Luding

Particle Technology, DelftChemTech, TU Delft, Julianalaan 136, 2628 BL Delft, The Netherlands, e-mail: [lui@ica1.uni-stuttgart.de](mailto:lui@ica1.uni-stuttgart.de) and [s.luding@tnw.tudelft.nl](mailto:s.luding@tnw.tudelft.nl)  
homepage: [www.ica1.uni-stuttgart.de/~lui](http://www.ica1.uni-stuttgart.de/~lui)

basic model for gases, liquids, and e.g. glasses [4]. Adding dissipation, friction and thus rotation to hard spheres, one has the simplest yet realistic model granulate. Disregarding eigenmodes of the grains and, to some extent, plastic deformation or breakage, one has Molecular dynamics (MD) simulations as an established tool to complement advanced theoretical approaches and experimental studies.

### 1.1

#### Freely cooling systems

Granular gases are the more dynamic limit of granular media as opposed to static systems. One of the outstanding effects in granular gases is the so called clustering, a self-stabilized density instability due to dissipation [5–7], where large, dense collections of particles co-exist with almost empty areas. Clustering occurs in initially homogeneous systems [5–9] and should not be confused with the so-called “inelastic collapse” [5], the divergence of the collision rate, which is inherent to the hard (rigid) sphere model [5, 6, 10, 11]. Freely cooling systems – mainly examined numerically and theoretically – are almost impossible to realize experimentally. Only in the last years, laboratory experiments were performed, where clustering could be examined in driven systems [12–18], where also kinetic theory approaches [19–27] complemented by numerical simulations have proven to be successful [10, 23, 28–33].

### 1.2

#### Driven systems

The driving of a granular material can be realized by moving walls [2, 34] which lead to local heating, or the system can alternatively be driven by a global homogeneous, random energy source in different variations [10, 23, 27, 31, 35–38]. The latter type of energy input does not exactly resemble the experimental situation, where a two-dimensional (2D) horizontal layer of spheres is agitated by vertical vibrations of the bottom surface and the horizontal degrees of freedom are indirectly agitated due to the different vertical jump heights of the colliding particles [13, 17, 18, 33]. Translational energy input (due to vibrations) was also applied for other boundary conditions and a variety of interesting experimental results were obtained just recently [12–15, 17, 18, 39].

Generic seems to be that one can obtain a gas and a liquid state, together with dense, solid-like clusters which form due to dissipation. Thus, the choice of the driving

term to put into a theory for dissipative systems is an open problem and we expect that it depends on the nature of the driving (vibrating wall, airflow, Brownian noise, etc.). In this paper we present a more detailed and complete study as in [10, 11] and also combine both approaches in the framework of a mean field theory for the evolution to the steady state.

We present a series of results from numerical simulations performed for different sizes  $N$  of the system, different values of  $r$  and different types of driving. The results are compared to an analytical MF approach.

### 1.3

#### Micro-Macro Transition

A straightforward approach towards the understanding of macroscopic material behavior by just modeling and simulating all atoms in a macroscopic system is not possible due to the huge number of degrees of freedom. Therefore, one can reduce the size of the examined system so that a microscopic simulation of atoms is possible. However, the possible length of such a “probe” is in general too small in order to regard it as macroscopic. Therefore, methods and tools to perform a so-called micro-macro transition [3, 40, 41] are discussed in this study. In a first step, microscopic simulations of a small sample lead to macroscopic laws needed to describe the material within the framework of a macroscopic theory, in a second step.

For granular materials, as an example, the grain properties are inserted into a discrete particle molecular dynamics (MD) and lead to the collective behavior of the dissipative many-particle system. From the particle simulation, one can extract, e.g., the pressure of the system as a function of density. This equation of state allows a macroscopic description of the material, which can be viewed as a compressible, non-Newtonian fluid [42]. Here we focus on the monodisperse hard sphere model which exhibits a disorder-order transition at a certain density. For low densities, the system resembles a dilute gas, for intermediate densities one has a disordered fluid, and for the highest densities, one obtains an ordered solid (evidenced by a crystal structure). The elastic hard spheres can be generalized by including inelasticity so that one ends up with a dissipative system for which, however, the micro-macro approach still can be applied.

From the algorithmic point of view, the model system is examined by an event-driven molecular dynamics simulation. One can compute the stress tensor and thus the pressure by summation over the momentum transfer per unit time and volume. In the usual time-driven molecular dynamics, the procedure is similar, only that forces have to be measured. The pressure can be derived for a dynamic system by means of kinetic-theory arguments [3], and for a quasi-static system by means of an average over particles [43] or by a virtual displacement method [40].

Examples are presented, where the above-described methods can be applied and where large-scale computation was used. Standard simulations involve  $10^4 - 10^5$  particles due to the efficiency of the event-driven algorithm and can be extended to much larger numbers by using parallelization and supercomputers [?].

### 1.4

#### Overview

The paper is organized as follows. Section 2 introduces and describes the model and the algorithm for numerical simulations. In section 3, the stress in a dense, elastic granular gas is examined, while in section 4, the model for frictional and driven systems is described. Thereafter, in section 5, mean field evolution equations for homogeneous driven systems are provided. The final example, freely cooling inhomogeneous gases are discussed in section 6, and a micro-macro transition for this system is shown in section 7. Section 8 contains a brief summary and conclusion.

## 2

### Model and Algorithm

In this section, the hard sphere model is introduced together with the event-driven algorithm. The generalized, so-called TC model takes into account a finite contact duration and, besides adding this physically relevant parameter to the model saves computing time.

#### 2.1

##### Hard Sphere Model

The particles are assumed to be perfectly rigid and follow an undisturbed motion until a collision occurs as described below. Due to the rigidity of the interaction, the collisions occur instantaneously, so that an event-driven simulation method [44, 45] can be used.

A change in velocity – and thus a change in energy – can occur only at a collision. The standard interaction model for instantaneous collisions of particles with radius  $a$ , mass  $m = (4/3)\pi\rho a^3$ , and material density  $\rho$  is used in the following. The post-collisional velocities  $\mathbf{v}'$  of two collision partners in their center of mass reference frame are given, in terms of the pre-collisional velocities  $\mathbf{v}$ , by

$$\mathbf{v}'_{1,2} = \mathbf{v}_{1,2} \mp (1+r)\mathbf{v}_n / 2, \quad (1)$$

with  $\mathbf{v}_n \equiv [(\mathbf{v}_1 - \mathbf{v}_2) \cdot \hat{\mathbf{n}}] \hat{\mathbf{n}}$ , the normal component of the relative velocity  $\mathbf{v}_1 - \mathbf{v}_2$ , parallel to  $\hat{\mathbf{n}}$ , the unit vector pointing along the line connecting the centers of the colliding particles. If two particles collide, their velocities are changed according to Eq. (1), with the change of momentum

$$\Delta\mathbf{P} = -m(1+r)\mathbf{v}_n / 2, \quad (2)$$

and the change of translational energy at a collision  $\Delta E = -m(1-r^2)v_n^2/4$ , with dissipation for restitution coefficients  $r < 1$ .

#### 2.2

##### The time driven, soft particle technique

Even without using the soft particle method [43, 46, 47] in this study, it is convenient to discuss briefly the standard approach. Replacing  $\Delta\mathbf{P}$  in Eq. (2) by  $\mathbf{f}(t)\Delta t_{MD}$ , with the molecular dynamics time step  $\Delta t_{MD}$ , allows the integration of the corresponding, discretized equations of motion with standard numerical methods [47].

Since the modeling of realistic deformations of the particles would be much too complicated, let us assume that the overlap of two particles is the only quantity important for the interaction potential. The interaction of two particles can be split into (at least) three independent forces, and is typically short range, i.e. the particles interact only when they are in contact. The first force, an elastic repulsive force proportional to the overlap, accounts for the excluded volume which each particle occupies. In the simplest case, a linear spring can be used. The second force, a viscous damping force, models the dissipation in the normal direction and is proportional to the relative velocity. The simplest possible dashpot is again linear. This linear spring-dashpot model can be solved analytically and leads to a constant contact duration  $t_c$  and a constant restitution coefficient  $r$  [48]. The third force, accounting for friction, acts in the tangential direction, but will not be discussed here; for more information see Refs. [2].

## 2.3

### The connection between hard- and soft-sphere models

In the ED method, the time during which two particles are in contact is implicitly zero. The consequence is that exclusively pair contacts occur and the instantaneous momentum change  $\Delta\mathbf{P}$  in Eq. (2) suffices to describe the collision. However, ED algorithms with constant  $r$  run into difficulties when the time between events,  $t_n$ , becomes too small – typically in systems with strong dissipation – and the so-called “inelastic collapse” occurs [45, 49], i.e. the collision rate diverges for a few particles in the system. Since this is an artefact of the hard sphere model, it is unphysical and has to be avoided. Because a diverging number of collisions is only possible if the contact duration vanishes, the physical contact duration  $t_c$  has to be reintroduced in order to allow for realistic ED simulations. In MD simulations, on the other hand, one has  $t_c > 0$ , since every contact takes some finite time. Therefore, only a limited amount of kinetic energy ( $\Delta E \propto 1 - r^2$ ) can be dissipated per collision. The finite contact duration implies a finite energy dissipation rate. In contrast, the consequence of a diverging collision rate would be a diverging energy dissipation rate.

In a dense system of real particles, energy dissipation becomes ineffective, i.e. the ‘detachment effect’ occurs [50, 51]. This effect is not obtained with hard particles and a constant coefficient of restitution  $r$ . Therefore, in the framework of the so-called TC model, the restitution becomes elastic in nature,  $r_n^{(i)} = 1$ , if collisions occur too frequently, i.e.  $t_n^{(i)} \leq t_c$ , for the collision  $n$  of particle  $i$ . The time since the last collision is  $t_n^{(i)}$  and the cut-off parameter  $t_c$  for elastic contacts can be identified with the contact duration. Thus, an additional material parameter is defined for the hard sphere model, that leads to qualitative agreement between ED and MD simulations and, in addition, avoids the inelastic collapse artefact. Recently, it has been shown that the TC model does not affect physical observables of the system, like the energy, as long as it is reasonably small [45].

## 2.4

### Event-Driven Algorithm

Since we are interested in the behavior of granular particles, possibly evolving over several decades in time, we use an event-driven (ED) method which discretizes the sequence of events with a variable time step adapted to the problem. This is different from classical MD simulations, where the time step is usually fixed.

In the ED simulations, the particles follow an undisturbed translational motion until an event occurs. An event is either the collision of two particles or the collision of one particle with a boundary of a cell (in the linked-cell structure) [47]. The cells have no effect on the particle motion here; they were solely introduced to accelerate the search for future collision partners in the algorithm.

Simple ED algorithms update the whole system after each event, a method which is straightforward, but inefficient for large numbers of particles. In Ref. [44] an ED algorithm was introduced which updates only those two particles which were involved in the last collision. For this a double buffering data structure is implemented, which contains the ‘old’ status and the ‘new’ status, each consisting of: time of event, positions, velocities, and event partners. When a collision occurs, the ‘old’ and ‘new’ status of the participating particles are exchanged. Thus, the former ‘new’ status becomes the actual ‘old’ one, while the former ‘old’ status becomes the ‘new’ one and is then free for the calculation and storage of possible future events. This seemingly complicated exchange of information is carried out extremely simply and fast by only exchanging the pointers to the ‘new’ and ‘old’ status respectively. Note that the ‘old’ status of particle  $i$  has to be kept in memory, in order to update the time of the next contact,  $t_{ij}$ , of particle  $i$  with any other object  $j$  if the latter, independently, changed its status due to a collision with yet another particle. During the simulation such updates may be necessary several times so that the predicted ‘new’ status has to be modified.

The minimum of all  $t_{ij}$  is stored in the ‘new’ status of particle  $i$ , together with the corresponding partner  $j$ . Depending on the implementation, positions and velocities after the collision can also be calculated. This would be a waste of computer time, since before the time  $t_{ij}$ , the predicted partners  $i$  and  $j$  might be involved in several collisions with other particles, so that we apply a delayed update scheme [44]. The minimum times of event, i.e. the times which indicate the next event for a certain particle, are stored in an ordered heap tree, such that the next event is found at the top of the heap with a computational effort of  $O(1)$ ; changing the position of one particle in the tree from the top to a new position needs  $O(\log N)$  operations. The search for possible collision partners is accelerated by the use of a standard linked-cell data structure and consumes  $O(1)$  of numerical resources. In total, this results in a numerical effort of  $O(N \log N)$  for  $N$  particles. For a detailed description of the algorithm see Ref. [44]. Using all these algorithmic tricks, we are able to simulate about  $10^5$  particles within reasonable time on a low-end PC [52], where the particle number is rather limited by memory than by CPU power.

### 3

#### The Stress in dense granular gases

As a first example, the stress in an elastic system of hard spheres is examined, and the micro-macro transition is performed in order to obtain the global equation of state of the system. The simplest contribution to the stress tensor is caused by the momentum transport due to the particle motion. This is the standard stress in an ideal gas, where the atoms (mass points) move with a certain fluctuation velocity  $\mathbf{v}$ . The kinetic energy  $E = \sum_{i=1}^N m v_i^2 / 2$  due to the fluctuation velocity  $v_i$  can be used to define the temperature of the gas  $k_B T = 2E/(DN)$ , with the dimension  $D$  and the particle number  $N$ . Given a number density  $n = N/V$ , the stress in the ideal gas is then isotropic and thus quantified by the pressure  $p = nk_B T$ . Note that  $k_B$  is dropped for the sake of simplicity in the following.

The additional contribution to the stress is due to collisions and contacts and will be derived from the principle of virtual displacement of soft interaction potentials and then modified for hard sphere systems.

#### 3.1

##### Stress from a Virtual Displacement

From the centers of mass  $\mathbf{r}_1$  and  $\mathbf{r}_2$  of two particles, we define the so-called branch vector  $\mathbf{l} = \mathbf{r}_1 - \mathbf{r}_2$ , with the reference distance  $l = |\mathbf{l}| = 2a$  and the corresponding unit vector  $\hat{\mathbf{n}} = \mathbf{l}/l$ .

The deformation in the normal direction, relative to a reference configuration, is defined as  $\Delta = \mathbf{l} - 2a\hat{\mathbf{n}}$ . A virtual change of the deformation is then

$$\delta\Delta = \Delta' - \Delta \approx \delta l = \boldsymbol{\epsilon} \cdot \mathbf{l}, \quad (3)$$

where the prime denotes the deformation after the virtual displacement described by the tensor  $\boldsymbol{\epsilon}$ .

The corresponding potential energy density due to the displacement of one pair of particles is  $u = k\Delta^2/(2V)$ , expanded to second order in  $\Delta$ , leading to the virtual change

$$\delta u = \frac{k}{V} \left( \Delta \cdot \delta\Delta + \frac{1}{2} (\delta\Delta)^2 \right) \approx \frac{k}{V} \Delta \cdot \delta l^n, \quad (4)$$

where  $k$  is the spring stiffness (the prefactor of the quadratic term in the series expansion of the interaction potential),  $V$  is the averaging volume, and  $\delta l^n = \hat{\mathbf{n}}(\hat{\mathbf{n}} \cdot \boldsymbol{\epsilon} \cdot \mathbf{l})$  is the normal component of  $\delta\mathbf{l}$ . (Note that, in first order,  $\delta u$  depends only on the normal component of  $\delta\Delta$  due to the scalar product with  $\Delta$ , which is parallel to  $\hat{\mathbf{n}}$ .)

From the potential energy density, we obtain the stress from a virtual deformation by differentiation with respect to the deformation tensor components

$$\boldsymbol{\sigma} = \frac{\partial u}{\partial \boldsymbol{\epsilon}} = \frac{k}{V} \Delta \otimes \mathbf{l} = \frac{1}{V} \mathbf{f} \otimes \mathbf{l}, \quad (5)$$

where  $\mathbf{f} = k\Delta$  is the force acting at the contact, and the dyadic product  $\otimes$  of two vectors leads to a tensor of rank two.

#### 3.2

##### Stress in Hard Sphere Systems

Combining the ideal gas contribution (momentum transport through translational motion) and the collisional contributions to the stress tensor [54], one has

$$\boldsymbol{\sigma} = \frac{1}{V} \left[ \sum_i m_i \mathbf{v}_i \otimes \mathbf{v}_i - \frac{1}{\Delta t} \sum_n \sum_j \mathbf{p}_j \otimes \mathbf{l}_j \right], \quad (6)$$

where  $\mathbf{p}_j$  and  $\mathbf{l}_j$  are the momentum change and the center-contact vector of particle  $j$  at collision  $n$ , respectively. The left sum runs over all particles  $i$ , the first right sum runs over all collisions  $n$  occurring in the time interval  $\Delta t$ , and the second right sum concerns the collision partners of collision  $n$  [45]. The force in Eq. (5) is thus replaced by the momentum exchange per unit time  $\mathbf{f} = \mathbf{p}_j/\Delta t$ .

#### 3.3

##### The Equation of State

The mean pressure  $p = (\sigma_1 + \sigma_2)/D$ , with the eigenvalues  $\sigma_1$  and  $\sigma_2$  of the stress tensor, for  $D = 2$  can now be obtained from simulations for different volume fractions [42, 54]. The dimensionless reduced pressure  $P = pV/E - 1$  contains only the collisional contribution and the two-dimensional simulations agree nicely with the theoretical prediction  $P_0 = 2\nu g_{2a}(\nu)$  [54], with the pair-correlation function  $g_{2a}(\nu) = (1 - 7\nu/16)/(1 - \nu)^2$ , and the volume fraction  $\nu = N\pi a^2/V$ , see Fig. 1. A small correction to  $P_0$ , based on a fit to the numerical data, is  $P_4 = P_0(1 - a_g\nu^4)$  with  $a_g = 0.1$ . The dimensionless pressure  $P$  is related to the collision rate  $t_n^{-1} = 4\nu g_{2a}(\nu)\sqrt{T/(\pi a^2 m)} = 2P\sqrt{T/(\pi a^2 m)}$  and the temperature. For a system with homogeneous, constant temperature, the collision rate is thus proportional to the dimensionless pressure  $t_n^{-1} \propto P$ .

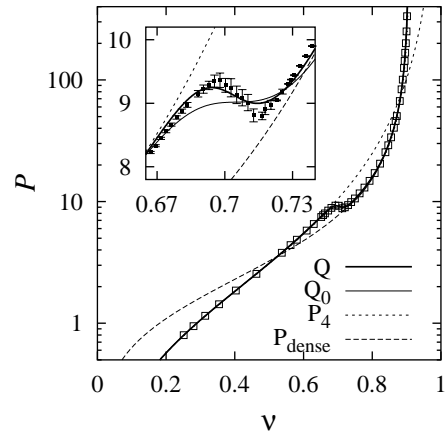


**Fig. 1.** The dashed lines are  $P_4$  and  $P_{\text{dense}}$  as a function of the volume fraction  $\nu$ , and the symbols are simulation data, with standard deviations as given by the error bars in the inset. The thick solid line is  $Q$ , the corrected global equation of state from Eq. (7) with the fit parameters  $a_g = 0.1$ ,  $a_d = 0.340$ ,  $a_p = 1.09$ ,  $\nu_c = 0.701$ ,  $\nu_{\max} = 0.9069$ , and  $m_0 = 0.00928$ . The thin solid line is  $Q_0$  without corrections, i.e.  $a_g = 0$ ,  $a_d = 0$ , and  $m_0 = 0.0015$  and  $\nu_c = 0.7$ , so that  $Q_0 = P_0 + m(\nu)[P_{\text{fv}} - P_0]$ .

When plotting  $P$  against  $\nu$  with a logarithmic vertical axis, in Fig. 1, the simulation results can not be distinguished from  $P_0$  for  $\nu < 0.65$ . Crystallization is evidenced at the point of the liquid-solid transition  $\nu_c \approx 0.7$ , and the data clearly deviate from  $P_0$ . The pressure is strongly reduced due to increase of free volume caused by order. The data diverge at the maximum packing fraction  $\nu_{\max}^{\text{mono}} = \pi/(2\sqrt{3})$  for a perfect triangular array. For high densities, one can compute from free-volume models, the reduced pressure  $P_{\text{fv}} = (\sqrt{\nu_{\max}/\nu} - 1)^{-1}$ , with the maximum volume fraction  $\nu_{\max}$  [54]. Slightly different functional forms do not lead to much better agreement [42]. Based on the numerical data, we propose the corrected high density pressure  $P_{\text{dense}} = [1 + a_d(\nu_{\max} - \nu)^{a_p}] P_{\text{fv}}$ , where the term in brackets [...] is a fit function with  $a_d = 0.340$  and  $a_p = 1.09$ .

To our knowledge, no theory exists, which combines the disordered and the ordered regime. Therefore, we propose a global equation of state

$$Q = P_4 + m(\nu)[P_{\text{dense}} - P_4], \quad (7)$$

with an empirical merging function

$$m(\nu) = [1 + \exp(-(\nu - \nu_c)/m_0)]^{-1} \quad (8)$$

which selects  $P_4$  for  $\nu \ll \nu_c$  and  $P_{\text{dense}}$  for  $\nu \gg \nu_c$  with the width of the transition  $m_0$ . In Fig. 1, the fit parameters  $\nu_c \approx 0.70$  and  $m_0 \approx 0.009$  lead to qualitative and quantitative agreement between  $Q$  (thick line) and the simulation results (symbols). However, a simpler version  $Q_0$  (thin line) without empirical corrections also leads to reasonable agreement when  $m_0 = 0.015$  is used. In the transition region, the function  $Q_0$  has no negative slope but is continuous and differentiable, so that it allows for an easy and compact numerical integration of  $P$ . We selected the parameters for  $Q_0$  as a compromise between the quality of the fit on the one hand and the treatability of the function on the other hand.

As an application of the global equation of state, the density profile of a dense granular gas in the gravitational field has been computed for monodisperse [54] and bidisperse situations [42]. In the latter case, however, segregation was observed and the mixture theory could not be applied.

## 4

### The model for frictional and heated systems

In this section the numerical model for driven systems is introduced, with a few typical examples of the simulation presented in Fig. 2.

A system of  $N$  three-dimensional spheres with radius  $a$  and mass  $m$  is considered, interacting via a hard-core potential and confined to a 2D plane of linear extension  $L$ , with periodic boundary conditions. The degrees of freedom are the positions  $\mathbf{r}_i(t)$ , the translational velocities  $\mathbf{v}_i(t)$ , and the rotational velocities  $\omega_i(t)$  for each sphere numbered by  $i = 1, \dots, N$ .

#### 4.1

##### Dissipation on collisions

The dissipation at a collision (in normal direction) is quantified by a constant normal restitution  $r$ . From the mo-

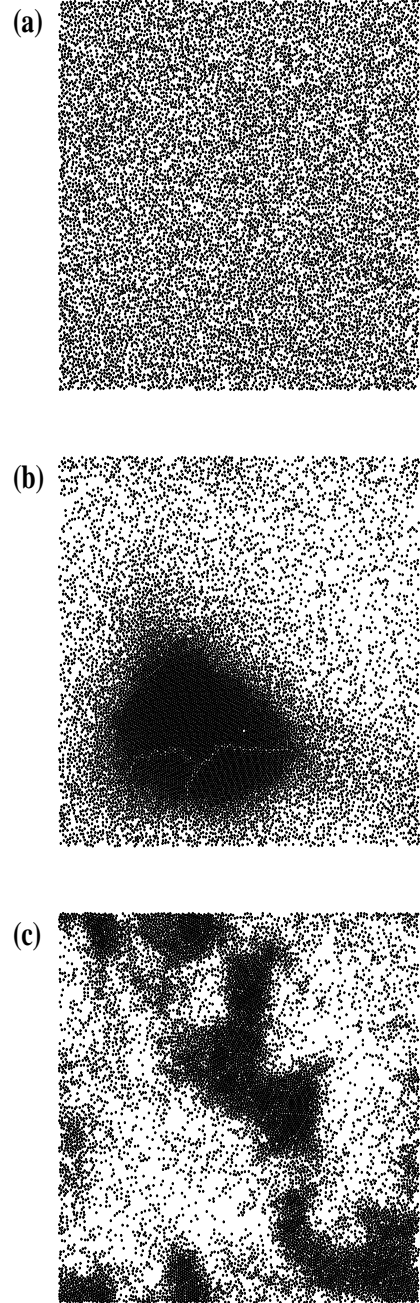


**Fig. 2.** Snapshots of the particle distribution in the steady state for a system of  $N = 11025$  smooth ( $r_t = -1$ ) particles,  $\delta = 1$ ,  $\nu = 0.34$ , and  $H_{\text{dr}} = 1.0 \text{ s}^{-1}$ , with  $r = 0.999$  (a),  $r = 0.97$  (b), and  $r = 0.6$  (c). In panel (d), a snapshot of the particle distribution in the steady state for a rotationally driven system of  $N = 11025$  particles,  $\nu = 0.34$ ,  $r_t = 1$ , and  $r = 0.1$  is shown for  $J = 1.0 \text{ s}^{-1}$ .

mentum conservation law and the rule  $\mathbf{v}'^{(n)}_c = -r\mathbf{v}^{(n)}_c$ , where the prime denotes the value after the collision, one can derive the change of linear momentum  $-(m/2)(1 + r)\mathbf{v}^{(n)}_c$  of particle  $i$ , which collides with particle  $j$ . The normal relative velocity is  $\mathbf{v}^{(n)}_c = [(\mathbf{v}_i - \mathbf{v}_j) \cdot \mathbf{n}] \mathbf{n}$ , and the unit vector in normal direction is  $\mathbf{n} = (\mathbf{r}_i - \mathbf{r}_j)/|\mathbf{r}_i - \mathbf{r}_j|$ .

In a similar way, the dissipation in tangential direction is quantified by the tangential restitution  $r_t$ , such that  $\mathbf{v}'_c^{(t)} = -r_t \mathbf{v}_c^{(t)}$ .

The magnitude of dissipation is proportional to  $1 - r^2$  (normal) and  $1 - r_t^2$  (tangential), while the strength of the coupling between rotational and translational motion is connected to  $1 + r_t$ , where the normal restitution  $r$  varies between 1 (elastic) and 0 (inelastic) and the tangential restitution  $r_t$  varies between  $-1$  (smooth) and  $+1$  (rough), corresponding to zero and maximum coupling, respectively [6, 9, 20, 55].

## 4.2

### Translational, multiplicative driving

The system is agitated each time interval  $\Delta t = f_{\text{dr}}^{-1}$ , with a driving rate  $f_{\text{dr}}$  (in the experiment this is according to the frequency of the vibrating bottom). For homogeneous driving, it is customary to assume  $f_{\text{dr}} \gg t_n^{-1}$ , where  $t_n^{-1}$  is the collision frequency of the granular gas. This, however, does not correspond to the experiments, were  $f_{\text{dr}}$  can be rather small [13, 17, 18]. In our simulations we will use driving frequencies around  $100 \text{ s}^{-1}$  comparable to those used experimentally [13, 17]. We did numerical checks with strongly different values of  $f_{\text{dr}}$  and found a similar behavior of the system even for driving frequencies lower than, but of the same order as  $t_n^{-1}$ , provided that a stationary state is reached.

Every time interval  $\Delta t$ , the velocity of particle  $i$  is changed:

$$\begin{aligned} v_i'^x(t) &= v_i^x(t) + r_i^x |\mathbf{v}_i(t)|^\delta v_r^{1-\delta} \\ v_i'^y(t) &= v_i^y(t) + r_i^y |\mathbf{v}_i(t)|^\delta v_r^{1-\delta}, \end{aligned} \quad (9)$$

where the driving occurs at time  $t$  and the prime on the left hand side indicates the value after the driving event.  $v_r$  is a reference velocity (in this study we use  $v_r = 1 \text{ m s}^{-1}$ ) which allows to define the dimensionless translational particle temperature  $T = E/(NT_r)$ , with  $E = (m/2) \sum_{i=1}^N \mathbf{v}_i^2$  and the reference temperature  $T_r = mv_r^2$ . The variance of the uncorrelated Gaussian random numbers  $r_i^x$  and  $r_i^y$  (with zero mean) can now be interpreted as a dimensionless driving temperature  $T_{\text{dr}}$ . The stochastic driving rule in Eq. (9) leads thus to an average rate of change of temperature

$$\Delta T / \Delta t = H_{\text{dr}} T^\delta \quad \text{with} \quad H_{\text{dr}} = f_{\text{dr}} T_{\text{dr}}. \quad (10)$$

In the next section we introduce this driving rate in the MF equation for the evolution of  $T$  [6], but first the case of rotational driving is discussed.

## 4.3

### Rotational driving

In the case of a rotational driving event, with frequency  $f_{\text{dr}}$ , see above, the translational velocity remains unchanged but the angular velocity  $\omega_i$  of particle  $i$  is modified at each time of agitation  $t$  so that

$$\omega'_i(t) = \omega_i(t) + r_i^\omega \omega_0, \quad (11)$$

where the prime on the left hand side indicates the value after the driving event. Due to the two-dimensionality

of the system, we apply the driving force only to the  $z$ -direction, so that the scalar  $\omega$  is to be understood as the  $z$ -component of  $\boldsymbol{\omega}$ .

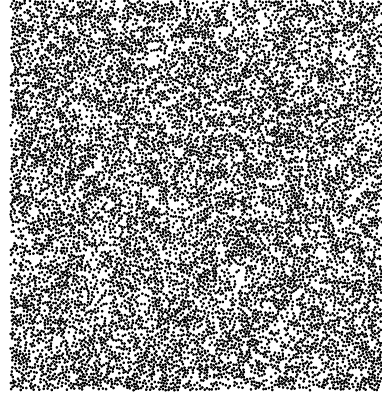


**Fig. 3.** Snapshot of the particle distribution in the steady state for a system of  $N = 11025$  smooth particles, with  $\nu = 0.34$ ,  $r_t = 1$ , and  $r = 0.1$  for  $J = 1.0 \text{ s}^{-1}$ .

The reference angular velocity,  $\omega_0$ , allows to define the dimensionless translational and rotational particle temperatures

$$T_{\text{tr}} = E_{\text{tr}} / (NT_0), \quad (12)$$

and

$$T_{\text{rot}} = 2E_{\text{rot}} / (NT_0), \quad (13)$$

with the translational energy  $E_{\text{tr}} = (m/2) \sum_{i=1}^N \mathbf{v}_i^2$ , the rotational energy  $E_{\text{rot}} = (qma^2/2) \sum_{i=1}^N \omega_i^2$  (with the moment of inertia prefactor  $q = 2/5$  for 3D spheres), and the reference temperature  $T_0 = mv_0^2$ , with  $v_0 = a\omega_0$ . The variance of the uncorrelated Gaussian random numbers  $r_i^\omega$  (with zero mean) can now be interpreted as a dimensionless driving temperature  $T_{\text{dr}}^\omega$  [11]. The stochastic driving leads thus to an average rate of change of temperature

$$\Delta T_{\text{rot}} / \Delta t = J_{\text{dr}}, \quad \text{with} \quad J_{\text{dr}} = f_{\text{dr}} T_{\text{dr}}^\omega. \quad (14)$$

In the case of driving of the translational degrees of freedom, the reference temperature  $T_r$  will be used, whereas in the case of rotational driving, the reference  $T_0$  will be used for scaling.

## 5

### Mean field evolution equations

The starting point for our mean-field analysis is the theory of Huthmann and Zippelius [9], for a freely cooling gas of infinitely rough particles, which was complemented by event driven (ED) simulations in 2D and 3D [6] and by studies of driven systems as well [10, 11]. The main outcome of this approach is a set of coupled evolution equations for the translational and rotational MF temperatures  $T_{\text{tr}}$  and  $T_{\text{rot}}$  [6, 9], which can be extended to describe arbitrary energy input (driving) [10, 11]. In the present study, given the random driving temperatures  $T_{\text{dr}}$  or  $T_{\text{dr}}^\omega$  and an energy input rate  $f_{\text{dr}}$ , as defined above, one just has to add

the positive rate of change of translational energy  $H_{\text{dr}}$  and rotational energy  $J_{\text{dr}}$  to the system of equations:

$$\frac{d}{dt}T_{\text{tr}}(t) = G \left[ -AT_{\text{tr}}^{3/2} + BT_{\text{tr}}^{1/2}T_{\text{rot}} \right] + H_{\text{dr}}T^{\delta}, \quad (15)$$

$$\frac{d}{dt}T_{\text{rot}}(t) = 2G \left[ BT_{\text{tr}}^{3/2} - CT_{\text{tr}}^{1/2}T_{\text{rot}} \right] + J_{\text{dr}}, \quad (16)$$

with

$$G = \frac{8\nu g_{2a}(\nu)}{a\sqrt{\pi m}}, \quad (17)$$

and the pair correlation function at contact  $g_{2a}(\nu) = (1 - 7\nu/16)/(1 - \nu)^2$  in the approximation proposed by Henderson and Verlet&Levesque [56, 57], dependent only on the volume fraction of the granular gas  $\nu = \pi a^2 N/V$ . The constant coefficients in Eqs. (15) and (16) are

$$A = (1 - r^2)/4 + \eta(1 - \eta)/2, \quad (18)$$

$$B = \eta^2/(2q), \text{ and} \quad (18)$$

$$C = \eta(1 - \eta/q)/(2q), \quad (19)$$

with the abbreviation  $\eta = \eta(r_t) = q(1 + r_t)/(2q + 2)$ , as derived and used in Refs. [6, 9].

Typical steady-state configurations for translational driving for different  $r$  values are shown in Fig. 2, and a snapshot for rotational driving is shown in Fig. 3.

### 5.1

#### Smooth particles – no rotation

The time evolution equation of  $T = T_{\text{tr}}$  was derived for the case of a freely cooling granular gas by means of a pseudo-Liouville operator formalism [6, 9]. We adopt the nomenclature and account for the driving by adding Eq. (10) to the mean field (MF) equation for the translational degree of freedom

$$\frac{d}{dt}T(t) = -G_r AT^{3/2} + H_{\text{dr}}T^{\delta}. \quad (20)$$

For our case of a homogeneous monolayer of smooth spheres, one has  $G_r = 8an\sqrt{\pi T_r/m}g(\nu)$ , and  $A = (1 - r^2)/4$ , with the number density  $n = N/V$ , the pair correlation function at contact  $g(\nu) = g_{2a}(\nu)$ , and the area fraction  $\nu$  covered by particles [6, 9, 10]. For  $\delta = 0$  the driving is homogeneous and independent of the local granular temperature (or velocity), and one can identify our energy input rate with the term  $m\xi_0^2$  in Ref. [58]. In the case  $\delta \neq 0$  the driving is a function of  $T$ . Imposing  $\frac{d}{dt}T(t) = 0$  one gets from Eq. (20) the MF temperature in the steady state

$$T^{\text{mf}} = \left( \frac{H_{\text{dr}}}{G_r A} \right)^{\frac{2}{3-2\delta}}, \quad (21)$$

the generalization of the Enskog equilibrium solution for a homogeneously driven granular gas [58]. The scaling exponent of  $T^{\text{mf}}$  in Eq. (21) is  $2/3$  for  $\delta = 0$ , while it is  $2$  for  $\delta = 1$ . For  $\delta \geq 3/2$  the MF theory does not admit a stable equilibrium state. If  $\delta > 3/2$  the driving rate grows faster than the dissipation rate.  $\delta = 3/2$  is a limiting case for which the equilibrium state is unstable against density fluctuations. A more detailed stability analysis is far from the scope of this paper, since the typical perturbation

around the steady state often also relies on a Maxwellian velocity distribution, which we do not find numerically.

The final approach to the steady state can be obtained by linearizing Eq. (20) around  $T^{\text{mf}}$ , what leads to an exponentially fast approach to equilibrium

$$T^{\text{mf}} - T(t+t_0) = T(t_0) \exp\{-[3At_n^{-1} + \delta H_{\text{dr}}(T^{\text{mf}})^{\delta-1}]t\}, \quad (22)$$

where  $t_n^{-1} = G_r \sqrt{T^{\text{mf}}}/2$  is the Enskog collision frequency for elastic particles with temperature  $T^{\text{mf}}$ , and  $T(t_0)$  is the initial temperature at time  $t_0$ . By inserting Eq. (21) in the expression for  $t_n^{-1}$ , one can express the characteristic relaxation time  $t_{\text{relax}} = [\dots]^{-1}$  as a function of the model parameters, which reduces for  $\delta = 1$  to  $t_{\text{relax}}^{-1} = (5/2)H_{\text{dr}}$ . Thus, for  $\delta = 1$  the characteristic time  $t_{\text{relax}} = [3At_n^{-1} + \delta H_{\text{dr}}(T^{\text{mf}})^{\delta-1}]^{-1}$  for the evolution of  $T$  towards its equilibrium value does *not* depend on  $A$  which contains all the information about the inelasticity. This characteristics is confirmed by numerical simulations (see below).

### 5.2

#### Rough particles with translational driving

Setting to zero the temporal derivatives in Eqs. (15) and (16), one obtains the steady state properties of the driven system with  $J_{\text{dr}} = 0$  and, for the sake of simplicity,  $\delta = 0$ :

$$T_{\text{rot}}^{\text{mf}} = \left( \frac{H_{\text{dr}}}{G\Gamma_{\text{tr}}} \right)^{2/3}, \text{ and } T_{\text{tr}}^{\text{mf}} = T_{\text{rot}}^{\text{mf}}/R, \quad (23)$$

with  $\Gamma_{\text{tr}} = (C/B^3)^{1/2}(CA - B^2)$ , and  $R = B/C$ .

Starting from this mean field result for both translational and rotational degrees of freedom, an analysis similar to the one in the previous subsection is possible. Since this did not lead to dramatically new insights, we do not discuss it further. Note, however, that the relaxation times for the translational and rotational degrees of freedom can be strongly different from each other [6].

### 5.3

#### Rough particles with rotational driving

Setting to zero the temporal derivatives in Eqs. (15) and (16), one obtains the steady state properties of the rotationally driven system with  $H_{\text{dr}} = 0$ :

$$T_{\text{rot}}^{\text{mf}} = \left( \frac{J_{\text{dr}}}{G\Gamma_{\text{rot}}} \right)^{2/3}, \text{ and } T_{\text{tr}}^{\text{mf}} = T_{\text{rot}}^{\text{mf}}/R, \quad (24)$$

with  $\Gamma_{\text{rot}} = 2(B/A^3)^{1/2}(CA - B^2)$ , and  $R = A/B$ . A more detailed analysis of this quasi steady state mean field solution, the approach to the steady state, the parameter dependencies, and the velocity distributions is to be published elsewhere.

### 5.4

#### Numerical simulations

Most of our event driven (ED) molecular dynamics simulations, see [6, 9–11] for details, with the driving specified above, are first equilibrated without driving and with elastic interactions ( $r = 1$ , and  $r_t = -1$ ), until the velocity

distribution is close to a Maxwellian. Then, dissipation and driving are switched on. However, we checked that the steady state does not depend on the initial conditions. The simulations are performed at a volume fraction  $\nu = 0.34$  with  $N = 1089$  ( $f_{\text{dr}} = 133 \text{ s}^{-1}$ ) or  $N = 11025$  ( $f_{\text{dr}} = 67 \text{ s}^{-1}$ ), and different values of  $r$  and  $r_t$ . (In our simulations with translational driving, we have chosen  $a = 10^{-3} \text{ m}$  and  $H_{\text{dr}} = 1.0 \text{ s}^{-1}$  so that, for example,  $G_r = 8\nu v_r / \sqrt{\pi} a g(\nu) = 3.1 \times 10^3 \text{ s}^{-1}$ ,  $T^{\text{mf}} = 0.0358$  and thus  $t_n^{-1} = 2.9 \times 10^2 \text{ s}^{-1}$ , if  $r = 0.90$  is used.) With these typical values and a homogeneous driving ( $\delta = 0$ ), the model of a driven granular gas is very close to a homogeneous state; no clusters are observed and the velocity distribution is almost Maxwellian. This is in contradiction to the experimental findings [13, 17], and suggests that the correct representation of the driving in those experiments is *not the homogeneous white noise* usually implemented.

#### 5.4.1 Approach to steady state

In Fig. 4 we compare the solution of the MF equation (21) for a multiplicative driving with  $\delta = 1$  to numerical simulations with  $N = 11025$ ,  $\nu = 0.34$ , and  $r = 0.99$ . As one can see, the transient dynamics is quite well reproduced by the MF theory, in the limit of low dissipation (quasi-elastic) considered in the simulations. In the steady state, intermittent behavior is evidenced, however, we do not present a more detailed statistical analysis here.

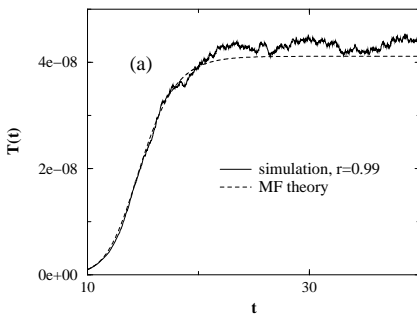


**Fig. 4.** Comparison between the solution of the MF equation (21) and numerical simulations for  $N = 11025$ ,  $\nu = 0.34$ ,  $\delta = 1$  and  $r = 0.99$ .

#### 5.4.2 Relaxation time

To check the prediction of the MF theory that the characteristic time  $t_{\text{relax}}$  is independent on  $A = (1 - r^2)/4$ , during the near-to-equilibrium relaxation to the steady state, different simulations with different  $r$  can be scaled. Because of noise and fluctuations in the initial conditions and dynamics with respect to the MF steady state, the simulation time  $t$  has to be translated by an offset time  $t_0$  in order to collapse the data from other realizations (data not shown here). The fact that the numerical data collapse

onto the MF curve, supports the MF prediction of the independence of the characteristic time from inelasticity in the case  $\delta = 1$ .

#### 5.4.3 Steady state temperature

In Fig. 5 we plot the ratio between the numerical results for long times  $T^{\text{eq}}$  and the theoretical equilibrium temperatures  $T^{\text{mf}}$  as function of  $r$  for different  $\delta$ . The agreement of the simulations with the MF prediction is optimal for  $r \rightarrow 1$ . For  $\delta < 0$ , the range of agreement extends to much smaller  $r$  values, i.e. to stronger dissipation, as in the case of  $\delta = 1$  and even in the case  $\delta = 0$ . One could naively think that the more negative is  $\delta$  the more favored should be the homogeneous state. In fact, this is not true. We have performed simulations with  $\delta = -1$ , and found that the driving is very singular in the low velocity limit, since an excessive amount of energy is given to slow particles.

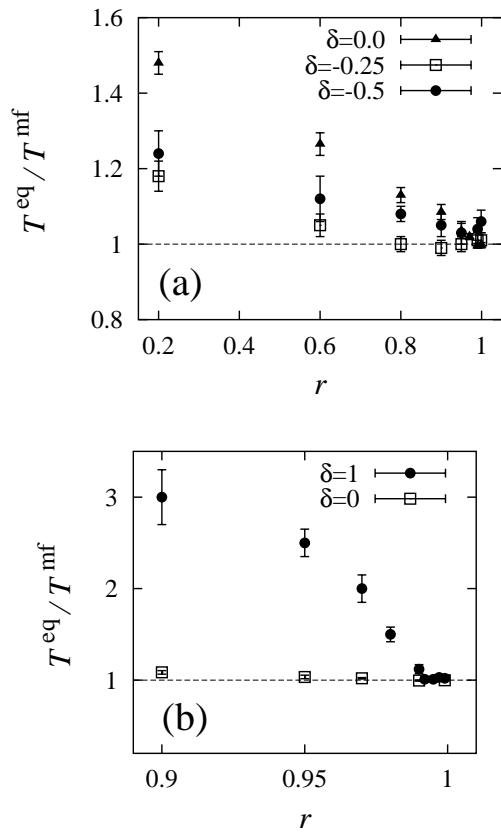


**Fig. 5.** Rescaled translational temperature  $T^{\text{eq}}/T^{\text{mf}}$  plotted against the restitution coefficient  $r$  for  $N = 11025$  and different values of  $\delta$  as given in the insets. Note the different axis scaling in (a) and (b).

#### 5.4.4

#### System size dependence

If the ratio between equilibrium temperature from simulations and MF temperature from the theory,  $T^{\text{eq}}/T^{\text{mf}}$ , is plotted against  $r$  for two system sizes  $N = 11025$  and  $5476$ , the data appear slightly different, indicating some size dependence. The deviation from unity, i.e. the discrepancy between theoretical prediction and numerical simulation of the model, is somewhat larger for the smaller system. For both system sizes, the quality of the theory is perfect in the limit  $r \rightarrow 1$ , within the statistical fluctuations.

#### 5.4.5

#### Steady state clustering

In Fig. 2 snapshots of the system's steady state were shown for  $r = 0.999$  (a)  $r = 0.97$  (b) and  $r = 0.6$  (c), for the more interesting case  $\delta = 1$ , rather than for the classical  $\delta = 0$ . Different regimes are observed: A homogeneous state exists for very weak dissipation ( $r = 0.999$ , Fig. 3, whereas dense, persistent clusters with a crystalline structure, domain boundaries, and vacancies are found for higher dissipation ( $r = 0.97$ ). The region between these clusters appears rather homogeneous and dilute (gas-like), very similar to the structures observed in experiments [13, 17]. For higher dissipation ( $r = 0.6$ ) the clusters appear less symmetric, are smaller, and evolve more dynamically.

Note that the clustering in the case  $\delta = 1$  is qualitatively different from the case of homogeneous driving, and it appears already for quite high values of  $r$  (see Fig. 2). Homogeneous driving, in fact, leads to transient clusters, i.e. they appear and disappear continuously, while in the experiments [13, 17] and in the case of multiplicative driving, the individual clusters are in equilibrium with a gas phase and are stable for rather long times. Simulations with negative  $\delta$ , (we used  $\delta = -0.5$  and  $\delta = -0.25$ ) give a behavior qualitatively similar to the case of homogeneous driving ( $\delta = 0$ ). For  $\delta = 1$ , the particles inside the cluster, with rather small relative velocities, are much less agitated than the particles in the surrounding gas phase, so that a cluster is stable. For  $\delta \leq 0$ , the particles in the cluster are driven comparatively strong, what leads to less stable, dynamic clusters.

#### 5.4.6

#### Simulations with rotation

In Fig. 6 we present the stationary (steady-state) values of  $T_{\text{rot}}$ , normalized by the MF value  $T_{\text{rot}}^{\text{mf}}(r = 0)$ , and of the ratios  $R = T_{\text{rot}}/T_{\text{tr}}$ , as obtained from numerical simulations and theory for a system of  $N = 11025$  particles, with volume fraction  $\nu = 0.34$ ,  $r_t = 1$ , and  $r$  ranging from  $0.99$  to  $10^{-4}$ . Surprisingly, the agreement with the MF prediction is very good, even for the lowest value  $r = 10^{-4}$  of the normal restitution, which corresponds to very strong dissipation, where the deviation from MF theory is of the order of only 10%.

To give an example, if the system is driven on the translational degrees of freedom, the stationary temperatures show deviations of 30 – 40% from MF predictions

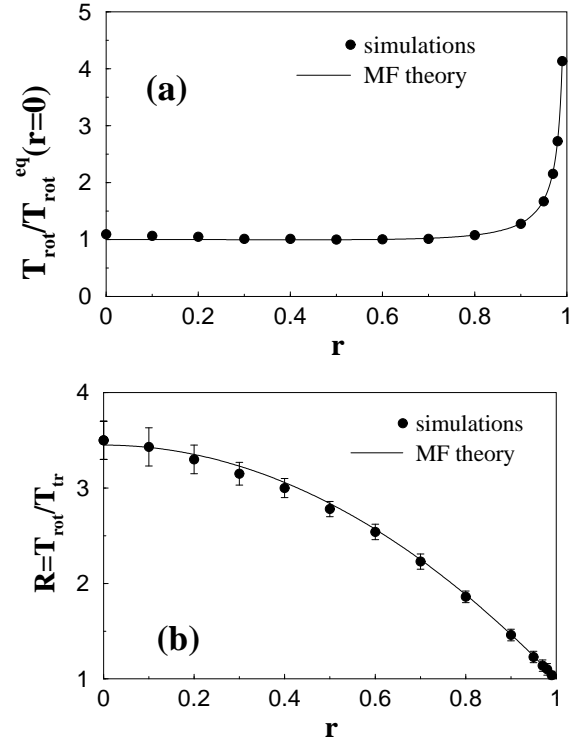


**Fig. 6.** Simulation (points) and theory (lines) for the parameters  $\nu = 0.34$ ,  $N = 11025$ , and  $r_t = 1$ , plotted against  $r$ . (a) Stationary rotational temperature  $T_{\text{rot}}$ , normalized by the MF value  $T_{\text{rot}}^{\text{mf}}(r = 0)$  at  $r = 0$ . (b) Ratio of stationary rotational and translational temperature  $R = T_{\text{rot}}/T_{\text{tr}}$ .

already for  $r = 0.6$ , see [10] and the previous section. The snapshot in Fig. 3 shows the particle distribution for  $r = 0.1$  and appears spatially homogeneous – apart from small density fluctuations not quantified here. Thus, rotational velocities are characterized by good homogenization at low  $r$ ; however, also the translational velocity distribution shows strong deviations from a Maxwellian as will be quantified in the next section. This deviation is due to the rather high dissipation. Numerical simulations with  $r = 0.99$  give a Maxwellian distribution for both rotational and translational velocities.

In order to check the role of the tangential restitution, we show in Fig. 7 the stationary values of  $R$  with  $r = 0.1$  and  $r_t \in [-1, 1]$ . While for positive  $r_t$  there is still good agreement with MF theory, strong deviations appear as  $r_t \rightarrow -1$ . Note that many realistic materials obey the relation  $r_t \approx 0.4$  [59], what renders our mean field approach still acceptable.

Our conclusions are that the driving on the rotational degrees of freedom is able to keep the spatial homogeneity of the system up to very high dissipation rates, for positive values of  $r_t$ . This leads to a very good agreement of the stationary temperatures with the MF predictions. There are two possible reasons for this. First, the driving acts on rotations. Then, it cannot favorize collisions, since it does not increase the normal component of the relative velocity of the colliding particles. Second, the increase of rotational energy triggered by the driving leads to a shearing force

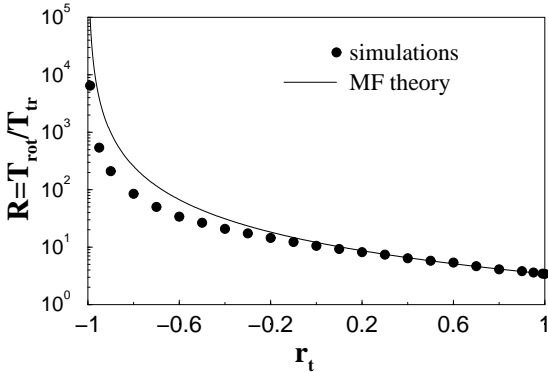


**Fig. 7.** Simulation (points) and theory (lines) results for  $R = T_{\text{rot}}/T_{\text{tr}}$ , with parameters  $\nu = 0.34$ ,  $N = 11025$ , and  $r = 0.1$ , plotted against  $r_t$ .

between particles, which reduces density fluctuations and should destroy the translational velocity correlations - but astonishingly does not. When  $r_t \rightarrow -1$ , i.e. in the smooth limit, the agreement with the MF is lost. To explain this result one has to remember that  $1 + r_t$  is a measure for the strength of the coupling. Not enough rotational energy is transferred to the translational degree, so that the randomization on collisions does not take place. Thus, it is not surprising that MF is no more valid in this very singular limit. Snapshots of the particle distribution for  $r = 0.1$  and  $r_t$  near to  $-1$  (not displayed here) show indeed stronger density fluctuations in the system as reported in Fig. 3.

## 5.5 Summary and Conclusions

The subject of this section was a granular gas subject to both translational driving *proportional* to a power  $\delta$  of the local velocity and to rotational driving (independent of the angular velocity). Numerical simulations and a theoretical analysis of this model for positive values of  $\delta$  reproduce qualitatively some experimental findings of [13, 17], which could not be accounted for by homogeneous driving ( $\delta = 0$ ). Furthermore, numerical simulations and theory for negative values of  $\delta$  and for rotational driving show good homogenization of the system up to very low values of the restitution coefficient,  $r$ , i.e. very strong dissipation.

A microscopic justification for the multiplicative driving is still lacking and requires more detailed experiments or three-dimensional simulation [33] studies. However, as suggested in [10], there is a possible experimental check of our ideas. From MF theory the scaling of the equilibrium temperature of the vertically vibrated gas with the area fraction  $\nu$  is given by  $T^{\text{mf}} \propto [\nu g(\nu)]^{-\frac{2}{3-2\delta}}$ . Experimental measurement of the equilibrium temperature of the vertically vibrated monolayer for different values of  $\nu$  could allow to estimate the value of  $\delta$  and to verify the hypothesis of a multiplicative effective driving.

Another result of the present study is that both the driving of the rotational degrees of freedom and a multiplicative driving with negative  $\delta$  are able to keep the spatial homogeneity of the system up to very high dissipa-

tation rates – at least for positive values of  $r_t$ , i.e. strong coupling between rotational and translational degrees of freedom. This leads to a very good agreement of the stationary temperatures with the MF predictions.

## 6

### Freely cooling granular media

The simulations presented in the following involve  $N = 99856 = 316^2$  dissipative particles with the restitution coefficients  $r = 0.8$ , in a periodic, quadratic system with volume fraction  $\nu = 0.25$ . The system size is  $l = Ld$  with dimensionless size  $L = 560$  and particle diameter  $2a = 1$  mm. In order to reach an equilibrated initial condition, the system is first allowed to equilibrate with  $r = 1$  for several hundreds of collisions per particle, so that a Maxwellian velocity distribution and a homogeneous density can be found. Then, at  $t = 0$  s, dissipation is activated and the quantities of interest are examined. Snapshots of the simulation with  $r = 0.8$  are presented in Fig. 8 at different, rescaled times  $\tau$  (see below).

The first picture in Fig. 8 is taken in the initially homogeneous cooling regime, whereas the next pictures show the different stages of the cluster growth regime. The final snapshot is taken in the limiting state, where the cluster has reached the system size. The particles are colored spots, where the green/red areas in the cluster centers correspond to particles with collision rate  $t_n^{-1} \geq 50 \text{ s}^{-1}$ . This is much smaller than the critical collision rate  $t_c^{-1} = 10^5 \text{ s}^{-1}$ , so that only a very small number of particles will be affected by the TC model.

## 6.1

### Homogeneous and inhomogeneous cooling

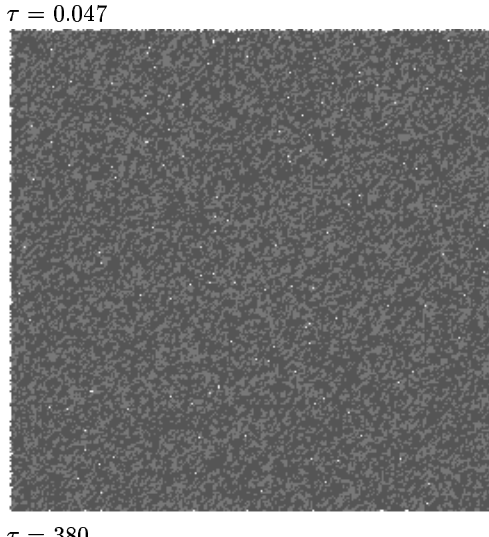
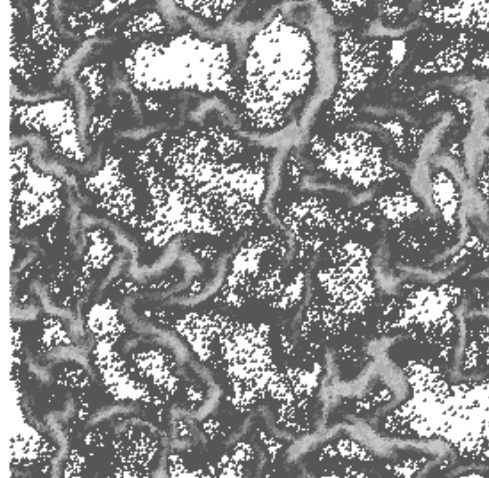
In the homogeneous cooling state [6, 8, 49], one can expect that the kinetic energy  $E = K(t)/K(0)$  of the system decays with time and follows the master-curve

$$E(\tau) = \frac{1}{(1 + \tau)^2}, \quad (25)$$

with the dimensionless time  $\tau = (1 - r^2)t/(4t_E)$ , the collision rate  $t_E^{-1} = 8\nu g(\nu)\bar{v}/(\sqrt{\pi}d)$ , the mean velocity  $\bar{v} = \sqrt{K(t)/Nm}$ , and the increased contact probability  $g(\nu) = (1 - 7\nu/16)/(1 - \nu)^2$  due to excluded volume effects at finite volume fractions  $\nu$ . Inserting the parameters from the simulation,  $1 - r^2 = 0.36$ ,  $g(\nu) \approx 1.5833$ , and  $\bar{v} = 0.02883 \text{ m/s}$ , one obtains an initial collision rate  $t_E^{-1}(0) = 51.5 \text{ s}^{-1}$ .

In Fig. 9, the normalized kinetic energy  $E$  is presented as a function of the normalized time  $\tau$ . At the beginning of the simulation we observe a perfect agreement between the theory for homogeneous cooling and the simulations. At  $\tau \approx 1-40$  substantial deviations from the homogeneous cooling behavior become evident, i.e. the decay of energy is slowed down earlier for stronger dissipation. The deviation from the analytical form increases until the clusters reach system size, when the behavior of  $E$  changes again to a slightly more rapid decrease.

This change in behavior is evident from the collision rate  $t_n^{-1}$  (data not shown here), see [7, 52]. At first, in the homogeneous cooling regime, the collision rate decays with

 $\tau = 380$  $\tau = 12150$ 

**Fig. 8.** ED simulation with  $N = 99856$  particles in a system of size  $L = 560$ , volume fraction  $\nu = 0.25$ , restitution coefficient  $r = 0.8$ , and critical collision frequency  $t_c^{-1} = 10^5 \text{ s}^{-1}$ . The collision frequency is grey-scaled, dark and light correspond to collision rates  $t_n^{-1} \approx 50 \text{ s}^{-1}$ , and  $2 \text{ s}^{-1}$ , respectively. The first image is homogeneous with the given density, however, due to the too large pixel size, the area appears covered.

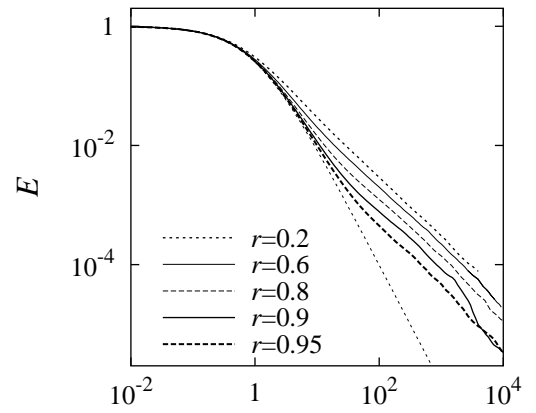


**Fig. 9.** (Left) Kinetic energy  $E$  plotted against  $\tau$  for different values of  $r$ . The dotted line represents Eq. (25).

$t_n^{-1} \propto \sqrt{E}$ . Then the collision rate is almost constant or even increases, until it becomes very noisy, indicating another change in the collective behavior, when the clusters reach system size. The long-time power law for the decay of energy with time is close to  $-2$  in the homogeneous cooling case. In the cluster growth regime, however, we obtain slopes slightly smaller than  $-1$  (the best fit leads to  $-0.920$ ,  $-0.927$ , and  $-0.941$  for  $r = 0.9$ ,  $0.8$ , and  $0.6$ , respectively, with errors  $\pm 0.002$ ).

## 6.2 Cluster growth

The cluster growth can be studied quantitatively in the spirit of reference [52]. All particle pairs with a distance smaller than some cut-off distance  $\delta < (1 + S)d$ , with an arbitrary cut-off parameter  $S = 0.1$ , are assumed to belong to the same cluster. After all particle pairs are examined, one obtains a cluster-size distribution and its moments. The first moment, the mean cluster size  $\langle M \rangle$ , and the size of the largest cluster  $M_{max}$  are plotted in Fig. 10 against the time  $\tau$ .

Both values are almost constant in the initial, homogeneous cooling regime. In the cluster growth regime a rapid increase of both  $\langle M \rangle$  and  $M_{max}$  is evidenced until, at larger  $\tau$ , the values reach a maximum and seemingly saturate or even decrease in the final regime where the clusters have reached system size. The cluster growth starts earlier for stronger dissipation, but the largest cluster seems to grow more rapidly for weaker dissipation, however, at a later time.

## 6.3 Discussion

With a rather simple description of a granular material as an ensemble of inelastic hard disks (spheres), we have investigated the interesting effect of clustering in freely cooling systems. For short times the system is disordered and gas-like, whereas the structures at larger times are dense, crystalline clusters. The clusters grow until they reach the system size. Simulations at very long times were

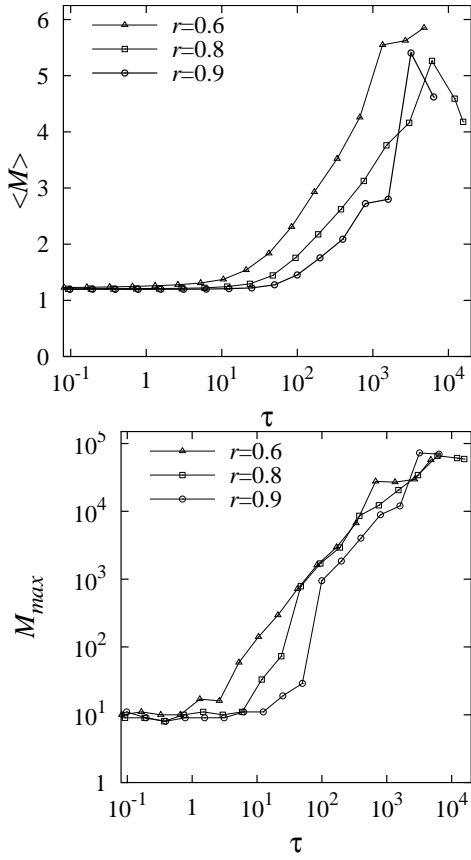


**Fig. 10.** (Left) Mean cluster size and (Right) maximum cluster size as functions of  $\tau$  for different coefficients of restitution  $r$ .

possible with the TC model, which reduces dissipation when contacts become too frequent.

Further investigations concerning the transport parameters pressure, viscosity and heat conductivity in similar systems are in progress in two dimensional model systems and are to be applied to a successful hydrodynamic theory of granular flow, as discussed in the following section.

## 7

### Micro-Macro Transition for a freely cooling system

In this section, from the ED simulations of a freely cooling dissipative gas [52] of hard spheres, field data are extracted. A rather large number of particles is necessary in order to allow for either good statistics or high resolution of patterns and structures for the micro-macro transition.

In order to obtain the fields from the simulation data, the system is arranged on a  $50 \times 50$  grid and the field quantities are computed for every cell. The density  $\nu(x, y) = n_c \pi a^2 / V_c$  and the fluctuation kinetic energy  $e(x, y) = (m/2) \sum_{i \in c} [\mathbf{v}_i - \mathbf{v}(x, y)]^2 / n_c$ , are plotted in Fig. 11. The symbols are the number of particles per cell  $n_c$ , the cell-volume  $V_c$ , the particle radius  $a$ , mass  $m$ , and the mean velocity  $\mathbf{v}(x, y) = \sum_{i \in c} \mathbf{v}_i / n_c$  in the cell. The iso-lines of the density are chosen such that the dilute area ( $\nu < 0.1$ ) is visible as well as the coexistence area between fluid and solid regions ( $0.6 < \nu < 0.8$ ). The islands ( $\nu > 0.8$ ) are solid clusters with triangular arrangement, whereas the is-

lands ( $\nu < 0.1$ ) are almost empty regions. Between pink and blue, the fluid phase exists at almost all densities.

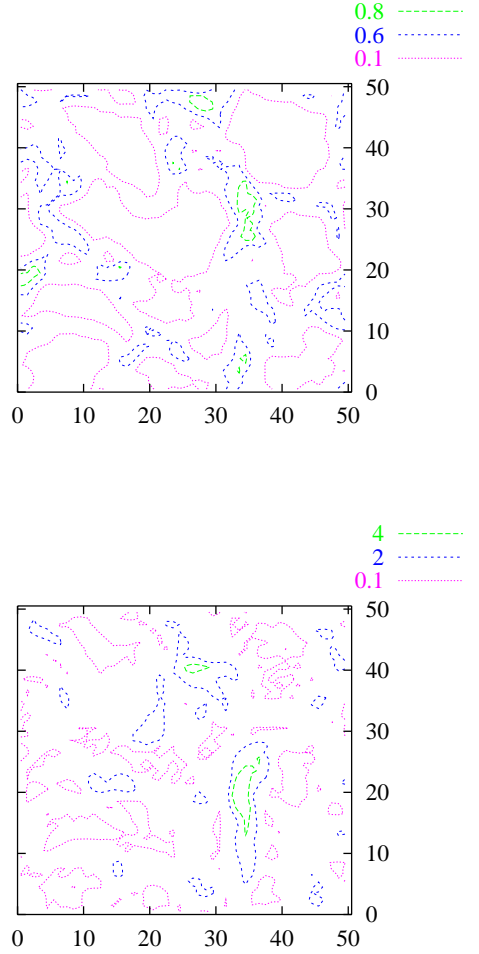


**Fig. 11.** Contour-plots of the density, temperature, and pressure fields on a  $50 \times 50$  grid. The values of the iso-lines are given in arbitrary units, for the latter two plots.

The iso-lines for the fluctuation kinetic energy are chosen in arbitrary units. However, it is evident, that the temperature and the density fields are not correlated in a simple fashion. Dense regions are not necessarily cold neither are dilute regions necessarily hot. The structure of the  $e$ -field appears more detailed than the structure of the density field.

Finally, the velocity vector field is plotted as momentum flux field in Fig. 12 and shows the mass-flux in the system. A closer examination leads to the conclusion that the clusters are not stable, but have remaining internal motion due to shear- or compressive modes. Note that also the velocity field (energy due to flux motion) is not directly correlated to the fluctuation kinetic energy.

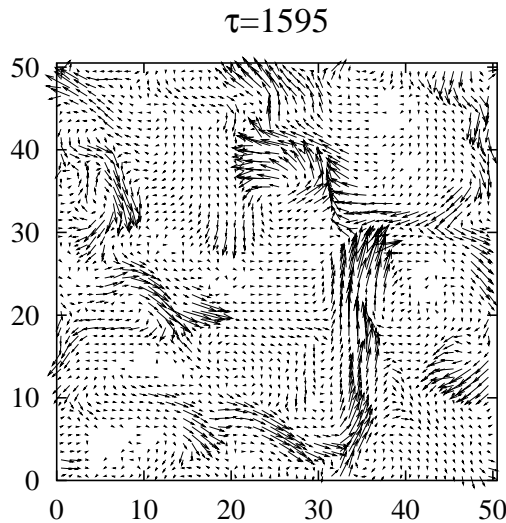


**Fig. 12.** Snapshot (top) of a system with  $N = 99856$  particles,  $r = 0.9$ , and  $\nu = 0.25$  together with the flux field (bottom) on a  $50 \times 50$  grid. The dimensionless time  $\tau$  roughly corresponds to the number of collisions per particle.

## 8

### Summary and Conclusion

As an example for granular media, hard sphere granular gases were examined by numerical simulations and theory in the spirit of a continuum theory, mainly for homogeneous systems. The systems studied involved freely cooling and driven two-dimensional granular gases with rotational degrees of freedom. The evolution of energy with time is nicely predicted by the theory for all cases examined so far, as long as the system remains homogeneous. When dissipation is strong enough, density variations build up and lead to clusters of particles. The deviation from the homogeneous theory goes ahead with the growth of these formations. Finally, a micro-macro approach was performed in order to obtain the density-, momentum-flux- and energy-fields in the framework of a continuum theoretical description – the latter is, however, not available yet.

In conclusion, theory and simulations show promising agreement in homogeneous systems, even for high densities or friction and rotations involved. The next step of current research is to understand also inhomogeneous, dynamic, non-equilibrium systems on the same level, also involving larger three-dimensional systems and more complicated boundary conditions.

### Acknowledgements

We acknowledge funding from the Deutsche Forschungsgemeinschaft (DFG) and thank all our collaborators in the cited papers that make up this review.

### References

- H. M. Jaeger, S. R. Nagel, and R. P. Behringer. Granular solids, liquids, and gases. *Reviews of Modern Physics*, 68(4):1259–1273, 1996.
- H. J. Herrmann, J.-P. Hovi, and S. Luding, editors. *Physics of dry granular media - NATO ASI Series E 350*, Dordrecht, 1998. Kluwer Academic Publishers.
- T. Pöschel and S. Luding, editors. *Granular Gases*, Berlin, 2001. Springer. Lecture Notes in Physics 564.
- K. R. Mecke and D. Stoyan, editors. *Statistical Physics and Spatial Statistics*, Berlin, 2000. Springer.
- I. Goldhirsch and G. Zanetti. Clustering instability in dissipative gases. *Phys. Rev. Lett.*, 70(11):1619–1622, 1993.
- S. Luding, M. Huthmann, S. McNamara, and A. Zippelius. Homogeneous cooling of rough dissipative particles: Theory and simulations. *Phys. Rev. E*, 58:3416–3425, 1998.
- S. Luding. Structures and non-equilibrium dynamics in granular media. *Comptes Rendus Academie des Science*, 3:153–161, 2002.
- P. K. Haff. Grain flow as a fluid-mechanical phenomenon. *J. Fluid Mech.*, 134:401–430, 1983.
- M. Huthmann and A. Zippelius. Dynamics of inelastically colliding rough spheres: Relaxation of translational and rotational energy. *Phys. Rev. E*, 56(6):6275–6278, 1998.
- R. Cafiero, S. Luding, and H. J. Herrmann. Two-dimensional granular gas of inelastic spheres with multiplicative driving. *Phys. Rev. Lett.*, 84:6014–6017, 2000.
- R. Cafiero, S. Luding, and H. J. Herrmann. Rotationally driven gas of inelastic rough spheres. *Europhys. Lett.*, 60(6):854–860, 2002.
- A. Kudrolli and J. P. Gollub. Studies of cluster formation due to collisions in granular material. In *Powders & Grains 97*, page 535. Rotterdam, 1997. Balkema.
- J. S. Olafsen and J. S. Urbach. Clustering, order and collapse in a driven granular monolayer. *Phys. Rev. Lett.*, 81:4369, 1998. cond-mat/9807148.
- W. Losert, D. G. W. Cooper, and J. P. Gollub. Propagating front in an excited granular layer. *Phys. Rev. E*, 59:5855, 1999.
- W. Losert, D. G. W. Cooper, J. Delour, A. Kudrolli, and J. P. Gollub. Velocity statistics in vibrated granular media. *Chaos*, 9(3):682–690, 1999. cond-mat/9901203.
- W. Losert, L. Bocquet, T. C. Lubensky, and J. P. Gollub. Particle dynamics in sheared granular matter. *Phys. Rev. Lett.*, 85(7):1428–1431, 2000. cond-mat/0004401.
- J. S. Olafsen and J. S. Urbach. Velocity distributions and density fluctuations in a 2d granular gas. *Phys. Rev. E*, 60:R2468, 1999.
- A. Prevost, D. A. Egolf, and J. S. Urbach. Forcing and velocity correlations in a vibrated granular monolayer. *Phys. Rev. Lett.*, 89:084301, 2002.
- J. T. Jenkins and S. B. Savage. A theory for the rapid flow of identical, smooth, nearly elastic, spherical particles. *J. Fluid Mech.*, 130:187–202, 1983.
- J. T. Jenkins and M. W. Richman. Kinetic theory for plane shear flows of a dense gas of identical, rough, inelastic, circular disks. *Phys. of Fluids*, 28:3485–3494, 1985.
- A. Goldshtain and M. Shapiro. Mechanics of collisional motion of granular materials. Part 1. General hydrodynamic equations. *J. Fluid Mech.*, 282:75–114, 1995.
- S. B. Savage. Analyses of slow high-concentration flows of granular materials. *J. Fluid Mech.*, 377:1–26, 1998.
- José María Montanero and Andrés Santos. Computer simulation of uniformly heated granular fluids. *Granular Matter*, 2(2):53–64, 2000. cond-mat/0002323.

24. I. Goldhirsch and T. P. C. van Noije. Green-Kubo relations for granular fluids. *Phys. Rev. E*, 61:3241–3244, 2000.
25. V. Garzó. Tracer diffusion in granular shear flows. cond-mat/0204268, 2002.
26. A. Barrat and E. Trizac. Lack of energy equipartition in homogeneous heated binary granular mixtures. *Granular Matter*, 4(2):57–63, 2002.
27. I. Pagonabarraga, E. Trizac, T. P. C. van Noije, and M. H. Ernst. Randomly driven granular fluids: Collisional statistics and short scale structure. *Phys. Rev. E*, 65(1):011303, 2002.
28. Y. L. Duparcmeur, H. J. Herrmann, and J. P. Troadec. Spontaneous formation of vortex in a system of self motorised particles. *J. Phys. I France*, 5:1119–1128, 1995.
29. A. Puglisi, V. Loreto, U. M. B. Marconi, and A. Vulpiani. Clustering and non-Gaussian behavior in granular matter. *Phys. Rev. Lett.*, 81:3848, 1998.
30. C. Bizon, M. D. Shattuck, and J. B. Swift. Linear stability analysis of a vertically oscillated granular layer. *Phys. Rev. E*, 60:7210–7216, 1999.
31. T. P. C. van Noije and M. H. Ernst. Velocity distributions in homogeneously cooling and heated granular fluids. *Granular Matter*, 1(2):57–64, 1998.
32. T. P. C. van Noije and M. H. Ernst. Velocity distributions in homogeneous granular fluids: the free and the heated case. cond-mat/9803042, 1998.
33. X. Nie, E. Ben-Naim, and S. Y. Chen. Dynamics of vibrated granular monolayers. *Europhys. Lett.*, 51(6):679–648, 2000. cond-mat/9910371.
34. S. McNamara and S. Luding. Energy flows in vibrated granular media. *Phys. Rev. E*, 58:813–822, 1998.
35. A. Puglisi, V. Loreto, U. M. B. Marconi, and A. Vulpiani. A kinetic approach to granular gases. *Phys. Rev. E*, 59:5582–5595, 1999.
36. C. Bizon, M. D. Shattuck, J. B. Swift, and H. L. Swinney. Velocity correlations in driven two-dimensional granular media. In J. Karkheck, editor, *Dynamics: Models and Kinetic Methods for Nonequilibrium Many-Body Systems*, pages 361–371, Dordrecht, 2000. Kluwer Academic Publishers. cond-mat/9904135.
37. T. P. C. van Noije, M. H. Ernst, and R. Brito. Spatial correlations in compressible granular flows. *Phys. Rev. E*, 57:R4891, 1998.
38. T. P. C. van Noije and M. H. Ernst. Randomly driven granular fluids: Large scale structure. *Phys. Rev. E*, 59:4326–4341, 1999.
39. A. Kudrolli and J. Henry. Non-Gaussian velocity distributions in excited granular matter in the absence of clustering. *Phys. Rev. E*, 62(2):R1489–92, 2000. cond-mat/0001233.
40. P. A. Vermeer, S. Diebels, W. Ehlers, H. J. Herrmann, S. Luding, and E. Ramm, editors. *Continuous and Discontinuous Modelling of Cohesive Frictional Materials*, Berlin, 2001. Springer. Lecture Notes in Physics 568.
41. J. G. Kirkwood, F. P. Buff, and M. S. Green. The statistical mechanical theory of transport processes. *J. Chem. Phys.*, 17(10):988, 1949.
42. S. Luding, M. Lätsel, and H. J. Herrmann. From discrete element simulations towards a continuum description of particulate solids. In A. Levy and H. Kalman, editors, *Handbook of Conveying and Handling of Particulate Solids*, pages 39–44, Amsterdam, The Netherlands, 2001. Elsevier.
43. M. Lätsel, S. Luding, and H. J. Herrmann. Macroscopic material properties from quasi-static, microscopic simulations of a two-dimensional shear-cell. *Granular Matter*, 2(3):123–135, 2000. cond-mat/0003180.
44. B. D. Lubachevsky. How to simulate billiards and similar systems. *J. of Comp. Phys.*, 94(2):255, 1991.
45. S. Luding and S. McNamara. How to handle the inelastic collapse of a dissipative hard-sphere gas with the TC model. *Granular Matter*, 1(3):113–128, 1998. cond-mat/9810009.
46. P. A. Cundall and O. D. L. Strack. A discrete numerical model for granular assemblies. *Géotechnique*, 29(1):47–65, 1979.
47. M. P. Allen and D. J. Tildesley. *Computer Simulation of Liquids*. Oxford University Press, Oxford, 1987.
48. S. Luding. Collisions & contacts between two particles. In H. J. Herrmann, J.-P. Hovi, and S. Luding, editors, *Physics of dry granular media - NATO ASI Series E350*, page 285, Dordrecht, 1998. Kluwer Academic Publishers.
49. S. McNamara and W. R. Young. Dynamics of a freely evolving, two-dimensional granular medium. *Phys. Rev. E*, 53(5):5089–5100, 1996.
50. S. Luding, E. Clément, A. Blumen, J. Rajchenbach, and J. Duran. Anomalous energy dissipation in molecular dynamics simulations of grains: The “detachment effect”. *Phys. Rev. E*, 50:4113, 1994.
51. S. Luding, E. Clément, A. Blumen, J. Rajchenbach, and J. Duran. Interaction laws and the detachment effect in granular media. In *Fractal Aspects of Materials*, volume 367, pages 495–500, Pittsburgh, Pennsylvania, 1995. Materials Research Society, Symposium Proceedings.
52. S. Luding and H. J. Herrmann. Cluster growth in freely cooling granular media. *Chaos*, 9(3):673–681, 1999.
53. S. McNamara and W. R. Young. Inelastic collapse in two dimensions. *Phys. Rev. E*, 50(1):R28–R31, 1994.
54. S. Luding, M. Lätsel, W. Volk, S. Diebels, and H. J. Herrmann. From discrete element simulations to a continuum model. *Comp. Meth. Appl. Mech. Engng.*, 191:21–28, 2001.
55. S. McNamara and S. Luding. Energy nonequipartition in systems of inelastic, rough spheres. *Phys. Rev. E*, 58:2247–2250, 1998.
56. D. Henderson. A simple equation of state for hard discs. *Mol. Phys.*, 30:971–972, 1975.
57. L. Verlet and D. Levesque. Integral equations for classical fluids. III. the hard disks system. *Mol. Phys.*, 46(5):969–980, 1982.
58. T. P. C. van Noije and M. H. Ernst. Ring kinetic theory for an idealized granular gas. *Physica A*, 251:266–283, 1998.
59. S. F. Foerster, M. Y. Louge, H. Chang, and K. Allia. Measurements of the collision properties of small spheres. *Phys. Fluids*, 6(3):1108–1115, 1994.
60. I. S. Aranson, B. Meerson, P. V. Sasorov, and V. M. Vinokur. Phase separation and coarsening in electrostatically driven granular media. *Phys. Rev. Lett.*, 88(20):204301, 2002.